Published in final edited form as:
Lab Chip. 2012 November 21; 12(22): 4855–4863. doi:10.1039/c2lc40306d.

A Novel Microfluidic Platform for High-Resolution Imaging of a Three-Dimensional Cell Culture under a Controlled Hypoxic Environment

Kenichi Funamoto[a,b], **Ioannis K. Zervantonakis**[c], **Yuchun Liu**[d,e,f], **Christopher J. Ochs**[f,g], **Choong Kim**[f,g], and **Roger D. Kamm**[b,c,f]

Kenichi Funamoto: funamoto@reynolds.ifs.tohoku.ac.jp; Roger D. Kamm: rdkamm@mit.edu

[a]Institute of Fluid Science, Tohoku University, Sendai 980-8577, Japan

[b]Department of Biological Engineering, Massachusetts Institute of Technology, Cambridge, MA 02139, USA

[c]Department of Mechanical Engineering, Massachusetts Institute of Technology, Cambridge, MA 02139, USA

[d]BIOMAT, Department of Mechanical Engineering, Faculty of Engineering, National University of Singapore, Singapore 117576, Singapore

[e]Experimental Fetal Medicine Group, Department of Obstetrics and Gynaecology, Yong Loo Lin School of Medicine, National University of Singapore, Singapore 119228, Singapore

[f]SMART BioSystems & Micromechanics (BioSyM), Singapore 117543, Singapore

[g]Division of Bioengineering, National University of Singapore, Singapore 117576, Singapore

Abstract

Low oxygen tensions experienced in various pathological and physiological conditions are a major stimulus for angiogenesis. Hypoxic conditions play a critical role in regulating cellular behaviour including migration, proliferation and differentiation. This study introduces the use of a microfluidic device that allows for the control of oxygen tension for the study of different three-dimensional (3D) cell cultures for various applications. The device has a central 3D gel region acting as an external cellular matrix, flanked by media channels. On each side, there is a peripheral gas channel through which suitable gas mixtures are supplied to establish a uniform oxygen

Correspondence to: Roger D. Kamm, rdkamm@mit.edu.

†Electronic Supplementary Information (ESI) available: Fig. S1: Contour map of oxygen tension at the center of the gel region on a glass cover slip in the microfluidic device without a film with a combination of Peclet numbers for media and gas flow, supplying 0% oxygen gas to both gas channels; Fig. S2: Variations of steady oxygen tension on a crosssection of the microfluidic devices with/without a film of a low diffusion coefficient of oxygen with a combination of Peclet numbers for media and gas flow; Fig. S3: Variations of oxygen tension profile across the middle of the gel region in the microfluidic device with the device thickness and diffusion coefficient of a film; Fig. S4: Transient change of oxygen tension on a crosssection of the microfluidic device with a film of low diffusion coefficient of oxygen; Fig. S5: Comparison of steady oxygen tension profiles across the gel region between the experiment and the corresponding numerical simulations; Fig. S6: 3D confocal rendering of tumor cell distribution in the device; Fig. S7: Live/dead assay of the cells in the cevice after 24-hr nomoxia/hypoxia; Fig. S8: Characterization of HIF-1α in the microfluidic device; Movie S1: The time-lapse images of migration of the MDA-MB-231 breast cancer cells for six hrs under normoxia and hypoxia. See DOI: 10.1039/b000000x/

concentration or gradient within the device. The effects of various parameters, such as gas and media flow rates, device thickness, and diffusion coefficients of oxygen were examined using numerical simulations to determine the characteristics of the microfluidic device. A polycarbonate (PC) film with a low oxygen diffusion coefficient was embedded in the device in proximity above the channels to prevent oxygen diffusion from the incubator environment into the Polydimethylsiloxane (PDMS) device. The oxygen tension in the device was then validated experimentally using a ruthenium-coated (Ru-coated) oxygen-sensing glass cover slip which confirmed the establishment of low uniform oxygen tensions (< 3%) or an oxygen gradient across the gel region. To demonstrate the utility of the microfluidic device for cellular experiments under hypoxic conditions, migratory studies of MDA-MB-231 human breast cancer cells were performed. The microfluidic device allowed for imaging cellular migration with high-resolution, exhibiting an enhanced migration in hypoxia in comparison to normoxia. This microfluidic device presents itself as a promising platform for the investigation of cellular behaviour in a 3D gel scaffold under varying hypoxic conditions.

Introduction

Oxygen tension is one of the most important factors influencing cell viability, migration, proliferation and differentiation. For instance, stem cells reside in a hypoxic niche, which regulates their cellular fate.[1] Hypoxia promotes proliferation of mesenchymal stem cells, while restraining their differentiation. It also enhances proliferation and differentiation of neural stem cells, while reducing cell death.[2, 3] In addition, hypoxia is a critical factor of the tumor microenvironment, with tumors exhibiting increased resistance to radiation therapy and certain anticancer drugs[4, 5] and enhanced metastasis of tumor cells by acute hypoxia.[6] These changes due to hypoxia are regulated by various proteins and their signalling processes, such as hypoxia-inducible factor-1 (HIF-1) and vascular endothelial growth factor (VEGF).[7]

Conventional gas variable incubators are most commonly used to study the effects of oxygen tensions on cell behaviours. These incubators create the desired oxygen environment by mixing oxygen, nitrogen and carbon dioxide in a predefined ratio. However, these systems do not allow the generation of oxygen gradients and are limited by the long times required for equilibrating the gas concentration.[8] Several groups developed platforms with gas microchannels attached to a cell culture well with a thin gas-permeable Polydimethylsiloxane (PDMS) membrane to generate a hypoxic environment.[9, 10] For example, Oppegard et al.[9] developed a device to control oxygen tension temporally (in minutes) and spatially (in millimetres) in a well plate commonly used for cell cultures. However, these devices are limited to two-dimensional cell culture studies. On the other hand, microfluidic systems are versatile tools to study cell behaviours with three-dimensional (3D) and real-time imaging at high-resolution.[11, 12] Due to the high level of control over the physical and chemical environment, these devices constitute the well-suited platform for the study of cell behaviour under the influence of various stimuli. These devices enable studies of migratory and proliferative behaviours of various cell lines when exposed to gradients of growth factors,[13, 14] temperature[15], interstitial flow[16], and interaction with multiple cell types[17–20]. Many microfluidic devices have also been reported to study the

effects of oxygen tension on cells or oxygen consumption by cells.[21–31] The designs commonly combine a media chamber, a gas-permeable membrane, channels for gas or oxygen scavenging reagents, and covers of PDMS or glass in order to create a uniform low oxygen tension.[25] Furthermore, oxygen gradients with an arbitrary profile were generated in microfluidic devices by mixing oxygen and nitrogen in gas channels dividing into multiple capillaries above a thin PDMS membrane.[22, 24, 28, 30] However, such microfluidic devices with several layers are complicated to fabricate, and there are difficulties in the accurate control of gas flow rates. Chen et al.[21] proposed a single-layer PDMS microfluidic device to generate oxygen gradients with the aid of spatially confined chemical reactions: oxygen scavenging/generating chemicals flow through two chemical reaction channels, which sandwiches a cell culture channel. But the microfluidic device utilized potentially cytotoxic chemicals, and the oxygen gradients created were nonlinear.

In this paper, we introduce a simple microfluidic device that allows the generation of low oxygen environments or an oxygen gradient for the study of cells in a 3D environment, using the flow of predefined harmless gas mixtures through channels in the device. Minimizing oxygen diffusion from the top surface of the microfluidic device is found to be essential for maintaining low oxygen tensions. The steady and transient oxygen tension in the device is numerically simulated under various conditions of media and gas flow rates. The oxygen tension in the microfluidic device is then correlated to the changes in fluorescent intensities of a Ru-coated oxygen-sensing glass cover slip bonded to the microfluidic channels. Finally, we demonstrate the utility of our novel device for studying the effect of hypoxic conditions on the migration characteristics of human breast cancer cells (MDA-MB-231).

Material and Methods

Device Design and Fabrication

Figure 1(a) represents the microfluidic device design and configuration. The device consists of a central channel of 1.3 mm width, into which a 3D extracellular matrix (ECM) such as collagen gel is injected. Flanking media channels of 500 μm width open out into a combined outlet port to avoid pressure differences across the gel region. Cells can be seeded in either the central channel or in the media channels, depending on the application of interest. Suitable gas mixtures are then infused into the other two peripheral channels of 500 μm width to establish an oxygen tension of interest or an oxygen gradient across the cell culture region. All channels have a height of 150 μm; the partitions between media and gas channels on both sides are set at 150 μm so as to ensure structural stability of the wall and allow for oxygen diffusion between the gas and media channels. The channel height allows observation of 3D cellular migration.

Fabrication procedure is depicted in a schematic diagram in Fig. 1(b). The microfluidic device was fabricated by first transferring the design to a 2 mm layer of PDMS by soft lithography (Step 1 in Fig. 1(b)). The PDMS (Silgard 184, Dow Chemical, MI, USA) was mixed at a 10:1 ratio of base:curing agent, poured over the silicon master, and incubated at 80 °C for at least 2 hrs. The cured PDMS layer was peeled off the silicon master, trimmed and placed on a petri dish (60 mm in diameter) with its patterned side facing the bottom. A

0.5 mm-thick polycarbonate (PC) film,[32, 33] which has a lower oxygen diffusion coefficient of 8.0×10^{-12} m^2/s than that of PDMS, was cut into a circular shape with a diameter of 35 mm. 3 mm port holes were punched at the locations of media, gas and gel ports, and positioned with the port holes on top of the corresponding ports on the solid PDMS layer. Subsequently, fresh PDMS was poured into the petri dish over the first PDMS layer to sandwich the PC film in the device (Step 2 in Fig. 1(b)). The final thickness of the microfluidic device was approximately 6 mm. The petri dish containing the device was placed in an oven at 80 °C overnight. The cured PDMS device was cut out from the petri dish and punched to form inlets and outlets of 2 mm in diameter for the infusion of media and gas, and 1 mm in diameter for the infusion of gel. Finally, the patterned side of the device and a glass cover slip were plasma treated (PDC-001, Harrick, CA, USA) prior to bonding (Step 3 in Fig. 1(b)).

Numerical Simulation of Oxygen Tensions in the Microfluidic Device

Numerical simulations were performed to investigate the oxygen tension in the device upon changing various parameters such as media and gas flow rates, device thickness, and effect of the PC film in the microfluidic device. The computational model of a 6-mm-thick microfluidic device, within which a 0.5 mm film is embedded at the 2 mm mark, was constructed for the parameter studies (Fig. 1(a)).

The media and gas flows through the individual channels were simulated by solving the Navier-Stokes equations and the equation of continuity. Both steady and transient oxygen tensions inside the device were calculated by solving the convection-diffusion equation. Simulations were performed by employing commercial finite element software (COMSOL Multiphysics 3.5a, COMSOL, MA, USA). The computational grid consisted of 120,000 – 140,000 tetrahedral elements. Media containing 21% oxygen was supplied from the two inlets, merging prior to reaching the single outlet port (Figs. 1(a) and (c)). Gas at 0% oxygen was supplied to both gas channels through the gas ports in order to establish a uniform oxygen tension. In another simulation study, (1–10% oxygen was supplied to the left-hand side') gas channel, and 21% oxygen to the right-hand side in order to create an oxygen gradient. Zero pressure and convection flux conditions were set at media and gas outlets, and a no-slip condition was applied on the channel wall for the fluid flow analysis. The parameter values used for density, viscosity, and diffusivity of oxygen in media[27, 28, 30], gel[34–36], gas, and PDMS[26, 37, 38] are summarized in Table 1. In addition, diffusivity in the embedded film, D_{film}, was assumed in a range of 2.0×10^{-9} m^2/s to 2.0×10^{-12} m^2/s, which corresponds to conditions in which the film is between two and 2,000 times less gas-permeable than PDMS, respectively. The Péclet number, the ratio of advection to diffusion, characterizes transport in the fluid flow:

$$Pe=Uw/D \quad (1)$$

where U is the average flow velocity in a channel, and w is the channel width of 500 μm. An increase of the value of Pe corresponds to an increased flow velocity, resulting in stronger convective transfer rates, relative to diffusion. In the simulations performed, the Péclet numbers of media and gas flows, Pe_m and Pe_g, were varied as 0, 1, 10, 100, and 1,000,

respectively, to optimize the media and gas flow rates for a desirable oxygen tension during cell culture (see Table 1).

Validation of Oxygen Tension

To experimentally validate the simulated oxygen tensions in the device, a sample of commercially available oxygen-sensing glass cover slip coated with Ru complex dye (FOXY-SGS, Ocean Optics, FL, USA)[9] was bonded to the bottom surface of the PDMS microfluidic device mold as previously described. For microscopic imaging, a digital CCD camera (C4742-95-12ER, Hamamatsu Photonics, Japan) connected to an inverted microscope (ECLIPSE TE300, Nikon, Japan) was employed. The oxygen-sensing glass cover slip was excited with green laser (λ_{ex} = 540–580 nm) and the fluorescence (λ_{em} = 595 nm) was recorded with a 4x magnification objective. Exposure time for brightness field and fluorescence imaging was set at 2 ms and 800 ms, respectively. The microscope image size was 1,344×1,022 pixels (2.18 mm × 1.66 mm).

The procedures of the validation experiment are summarized in Table 2. Since collagen type I gel was difficult to stabilize on the oxygen-sensing cover slip, leaking to the media channels easily, it was replaced by water in the validation experiment. Air was bubbled through water overnight to become saturated with 21% oxygen tension; this saturated water was added into the media channels and the gel region of the microfluidic device. The two inlets and one outlet of the media channels were connected to a reservoir, containing water treated in the same manner, and a syringe pump (EW-74901-00, Cole-Parmer, IL, USA), respectively (Fig. 1(c)). Water was withdrawn at a flow rate corresponding to Pe_m = 10 (10.8 μl/h for each media channel), while blocking the gel ports so as not to cause water flow in the gel region and to prevent evaporation during the experiment. Humidified gas mixture containing 21% oxygen, 5% carbon dioxide and 74% nitrogen (Airgas East Inc., MA, USA) was supplied to both gas channels at the flow rate of Pe_g = 100 (18 ml/min) to calibrate the device at 21% oxygen. Fluorescence images of the gel region were captured after 30 min of thermal and convective equilibrium (procedure 1 in Table 2). Then, the gas mixture was switched to the one containing 0% oxygen, 5% carbon dioxide and 95% nitrogen (Airgas East Inc., MA, USA) at the same flow rate to establish a low uniform oxygen tension in the device. The 0% oxygen gas mixture was humidified using a solution containing 10 wt% sodium sulfite (Na_2SO_3) to remove any dissolved oxygen. Fluorescence images were recorded every five min for the first 30 min, followed by every 30 min for three hrs, and six and 12 hrs after changing the gas supply (procedure 2 in Table 2). After that, the gas mixture on the right-hand side was switched to one containing 21% oxygen again to generate an oxygen gradient, and the fluorescence images were taken in the same manner for 12 hrs (procedure 3 in Table 2). Finally, the water in the media channels and the gel region was substituted with 10 wt% Na_2SO_3 solution, and gas flow with the same 0% oxygen gas was supplied through both gas channels without any media flow (Pe_m = 0). After allowing sufficient time for thermal and diffusive equilibrium and chemical reaction of scavenging oxygen (> 30 min), a fluorescence image was taken for the calibration of 0% oxygen tension (procedure 4 in Table 2).

The fluorescence intensity in each image was quantified using image processing software (ImageJ, NIH, MD, USA). Three fluorescence intensity profiles across the media channels and gel region were obtained by setting three rectangular regions of interest (ROI) of 1,276×80 pixels (2 mm × 0.13 mm). Each ROI was divided into small sections of 0.1 mm × 0.13 mm, and the space-averaged fluorescence intensity in each section was obtained. Then, the fluorescence intensity in each condition was converted to an oxygen tension based on the Stern-Volmer equation:[21]

$$\frac{I_0}{I}=1+K_q[O_2] \quad (2)$$

where I and I_0 are the fluorescence intensities in oxic and anoxic atmospheres, respectively. The quenching constant, K_q, is defined as follows:

$$K_q=\frac{I_0}{I_{100}}-1 \quad (3)$$

where I_{100} is the fluorescence intensity in 100% oxygen tension. For the calibration, the fluorescence intensities, I_{21} and I_0, in 21% and 0% oxygen tension conditions measured before and after the sequential experiments, respectively, were used. In this case, the quenching constant, K_q, can be described by changing Eqs. (2) and (3):

$$K_q=\frac{I_0-I_{21}+I_{21}[O_2]_{air}}{I_{21}[O_2]_{air}}-1 \quad (4)$$

where $[O_2]_{air}$ is 21%. The validation experiment was performed three times, using three microfluidic devices, to check the reproducibility.

Cell Migration Study under Hypoxia

The feasibility of the microfluidic device for cellular experiments was examined by monitoring the migration of GFP-labelled MDA-MB-231 human breast cancer cell line (generously provided by Prof. D. Lauffenburger, MIT) under normoxia and hypoxia. The MDA-MB-231 cells were passaged in standard Dulbecco's Modified Eagle Medium (DMEM) (Invitrogen, CA, USA) supplemented with 10% fetal bovine serum (FBS) (Invitrogen, CA, USA) and cultured in a humidified incubator at 5% CO_2 and 37 °C. Cells were collected by trypsinization and mixed into 1.5 mg/ml collagen type I gel to a final cell density of 0.5 million cells/ml. Collagen gel solution was introduced into the gel region of the microfluidic device and polymerized in an incubator for 45 min prior to adding DMEM/FBS media containing 50 ng/ml EGF (PeproTech, NJ, USA). After 24 hrs of culture, the microfluidic device was set on the stage of a time-lapse imaging system, equipped with an inverted microscope (Axiovert 200, Carl Zeiss MicroImaging(2-8) GmbH, Germany) and digital image processing software (AxioVision, Carl Zeiss MicroImaging GmbH, Germany), inside an environmental chamber to maintain a humidified atmosphere of 5% CO_2 and 37 °C. The following procedures of the cellular experiment are summarized in Table 2. A gas mixture containing 21% oxygen, 5% carbon dioxide and 74% nitrogen was supplied at a flow rate corresponding to Pe_g = 100 through each gas channels to create a

normoxic condition. No media flow was applied in this study. After thermal equilibrium of the device (> 30 min), both bright field and fluorescence images were taken at 10x magnification every 10 min for > 8 hrs (procedure A in Table 2). Hypoxia was then generated by switching the gas mixture from 21% oxygen gas mixture to 0% oxygen gas mixture through both gas channels. Microscope images were taken every 10 min for > 8 hrs to monitor cell migration (procedure B in Table 2).

Cancer cell migration > 2 hrs after supplying each gas mixture in the fluorescence microscope images was tracked for six hrs. The Imaris software (Bitplane, CT, USA) was used to analyze net cell displacement (distance between initial and final cell positions), total path length (total trajectory length obtained by summing all trajectory segments) and their ratio (persistence) as defined previously.[39] The results of 35 randomly selected cells were averaged in each condition, and three sets of the data with three devices were used to evaluate the significant differences between cell migration under normoxia and hypoxia by a Student's *t*-test. The differences were considered significant at $P < 0.05$. Tumor cells were fixed with 4% Paraformaldhyde, permeabilized with 0.1% Triton-X and stained for DAPI (Invitrogen, CA, USA) and mouse anti-human HIF-1α (clone H1alpha67, Abcam, MA, USA) detected with a secondary Alexa568 anti-mouse antibody (Invitrogen, CA, USA). To quantify expression of HIF-1α, we used ImageJ and measured the mean fluorescent intensity per cell in the nucleus for at least 10 cells per condition using the method described in the reference.[40]

Cell viability was checked after > 8 hrs culture inside the device under normoxia/hypoxia using LIVE/DEAD Cell Imaging Kit (488/570, Molecular Probes, Life Technologies Corp., CA, USA).

Results and Discussion

Characteristics of Oxygen Tension in the Microfluidic Device

Oxygen distribution inside the microfluidic device was simulated by solving the governing equations for both steady and transient oxygen tensions. The effects of media and gas flow rates on oxygen concentration were examined.

The oxygen tension at the centre of the gel region on the glass cover slip, $(x, y, z) = (0\ \text{m}, 1.975\times10^{-3}\ \text{m}, 1\times10^{-6}\ \text{m})$ (see Fig. 1(a) for location of *xyz* coordinate axes) in the microfluidic device with a film of $D_{\text{film}} = 2.0\times10^{-12}\ \text{m}^2/\text{s}$ was obtained from each computational result. Figures 2(a) summarizes the variation of the oxygen tension with a combination of Péclet numbers for media and gas flow. Oxygen tension increased with increasing media flow, Pe_{m}, since the medium is convected downstream before it has a chance to equilibrate with gases diffusing from the gas channels. On the other hand, gas flow, Pe_{g}, exerts little effect on oxygen tension, at least the range tested. The combination of the media and gas flow rate at $(Pe_{\text{m}}, Pe_{\text{g}}) = (10, 100)$ was found to be sufficient to achieve ~2% oxygen tensions, and was used for all further simulations. The oxygen tension at the same location in the microfluidic device without the film is represented in ESI (Fig. S1). The efficiency of the film is evident in a comparison of Figs. 2(a) and S1. Without the film, the lowest oxygen tension attainable is 6.5%.

Figure 2(b) shows the representative computational results of oxygen tension on the glass cover slip of the microfluidic device with/without the film at (Pe_m, Pe_g) = (10, 100) for a hypoxic reasonably uniform oxygen tension or a gradient of oxygen tension. Upon appropriate combinations of media and gas flow rates, a uniform oxygen tension along the gel region can be maintained. Contours of oxygen tension in the other conditions are shown in the ESI (Fig. S2). Oxygen tension profiles along a line across the media channels and gel region, (y, z) = (1.975×10^{-3} m, 1×10^{-6} m), are extracted in Fig. 2(c). In the case of gas flow through both channels, the microfluidic device with a film gives a more uniform oxygen tension profile in the gel region than that without the film, showing the significant influence of ambient oxygen diffusion on uniformity of oxygen concentration. The device with an embedded film also exhibited a more linear gradient of oxygen tension from 15% on right-hand side to 8% on the left-hand side of gel region, in the gradient case, demonstrating the beneficial effect of the PC film.

The thickness of the microfluidic device also affected the oxygen tension as oxygen readily diffuses through the PDMS.[41] Oxygen tension in the device without the film decreased with increasing device thickness (Fig. S3(a)). However, the oxygen tension became independent of thickness when the device thickness exceeded ~10 mm, and ~5% oxygen concentration remained at the centre of the gel region, due primarily to oxygen diffusion through the sides of the device. The oxygen tension in the microfluidic device was further decreased upon embedding a gas-impermeable film. The efficiency of a film was also investigated by changing the diffusion coefficient of oxygen through the film. By decreasing the diffusion coefficient (e.g., by the use of different materials), the steady oxygen concentration can be further reduced, but only for the values of $D_{film} \geq 2.0\times10^{-11}$ m^2/s, becoming constant thereafter (Fig. S3(b)).

The transient response to the supply of gas under 0% oxygen conditions was evaluated by observing the oxygen tension on a glass cover slip at the centre of the gel region in the device (Fig. 2(d), distributions shown in Fig. S4). In the first 600 s, the two devices with and without the gas-impermeable film have nearly the same oxygen tension. After that, the oxygen tension in the device with the film further decreases to less than 5% after 30 min, the difference being due to oxygen diffusion through the upper surface of the PDMS.

Experimental Validation of Oxygen Tensions in the Microfluidic Device

Oxygen tension was measured based on changes in fluorescence intensity indicated by a Ru complex coated oxygen-sensing glass cover slip bonded to the bottom of the microfluidic device. The actual microfluidic device used in the validation experiment had a 7.2 mm thickness on average, and the PDMS thickness below the PC film was ~2.75 mm.

Figure 3(a) shows microscope images of the microfluidic device. In the bright field image, the central gel region flanked by media channels and PDMS pillars to contain the gel are displayed. The corresponding fluorescence image under normoxia at 21% oxygen tension (21%-21%) was dark though several white dots were observed due to imperfections in the Ru-coating on the oxygen-sensing glass cover slip. The fluorescence intensity increased after supplying 0% oxygen gas through both gas channels (0%-0%), indicating oxygen tension decreased. The oxygen-sensing glass cover slip was first calibrated by using

intensities with two known oxygen tensions of 21% and 0% (see Fig. 3(a)), and the quenching constant, K_q, was obtained by Eq. (4). Then, the oxygen tension profile for each condition was computed using the Stern-Volmer equation of Eq. (2). Figure 3(b) shows a representative transient change of compensated fluorescence intensity profile or oxygen tension across the media channels and the gel region in the case of uniform hypoxia, indicating that > 3 hrs are needed to reach a steady state. Steady oxygen tension profiles in the cases of a uniform low oxygen tension and an oxygen gradient are summarized in Fig. 3(c). A uniform hypoxia condition with < 3% oxygen tension and an oxygen gradient from 16% on right-hand side to 10% on the left-hand side of gel region was established experimentally in the microfluidic device.

Compared to the numerical simulation results, the levels of measured oxygen tension were as low as in the simulation, especially in the case of uniform oxygen tension (Figs. 3(c) and S5). However, the reduction of oxygen tension achieved took slightly longer than simulated. The discrepancy between the measurement and the numerical simulation could possibly be attributed to non-ideal device fabrication and setup errors, resulting in diffusion of atmospheric oxygen through the gas ports and the flow devices, such as tubing, flowmeters and humidifier bottles. Perhaps the greatest source of uncertainty is due to the effects of imperfect bonding of the PC film to PDMS. Uncertainties might also arise in specifying some of the parameters of the simulation and in the boundary conditions (e.g., the gas tensions of the incoming fluids) that could account for the observed differences. Finally, substitution of water for collagen type I gel could lead to small convective flows within the gel region and affects the oxygen tension, especially in the gradient case.

Cancer Cell Migration under Hypoxia

Hypoxia is known to promote metastasis of a certain tumor cell type, associated with resistance to anti-cancer drug and radiation therapy, and enhancing their invasive potential.[4–6] Since our microfluidic device is designed for 3D and real-time imaging of cells in either the gel or media channels under hypoxia, cancer cell behaviour can be observed in detail. To demonstrate the utility of the microfluidic device, we investigated the migrations of MDA-MB-231 breast cancer cells under normoxic and hypoxic conditions, by supplying a 21% and 0% oxygen gas mixture through the two gas channels, respectively, in separate experiments. The microfluidic device design enabled us to monitor the cell trajectories at high spatial resolution in real-time (Movie S1). To demonstrate the advantage of our device to study tumor cell migration in a 3D environment, 3D confocal images of tumor cells seeded in the device were obtained (Fig. S6). Compared to 2D assays, cell migration in 3D is more relevant to tumor progression and involves cellular processes such as traction and proteolysis.[42] Furthermore, hypoxic conditions promote over expression of matrix remodelling enzymes[43], therefore 3D ECM migration assays are critical for investigating the effects of hypoxia in realistic settings. Culture media was not evaporated during the course of the experiment. Live/dead assay of the cancer cell showed that 89% cells were alive after > 8 hrs hypoxia (Fig. S7). Hence, cells were viable in the microfluidic device.

Representative migration trajectories of 35 randomly selected cells are shown in Fig. 4(a) under normoxic and hypoxic conditions. We quantified the net displacement, total path

length and their ratio (persistence) for all cell trajectories as defined by Fig. 4(b), and found that these two migration metrics increased upon culture under hypoxic condition, showing significant differences with the *P* values of 0.016 and 0.023, respectively (Fig. 4(c)). Interestingly, hypoxic conditions promoted directional cell migration compared to normoxic conditions, as indicated by the higher persistence values (see Fig. 4(b)). This increased invasive behaviour of MDA-MB-231 cancer cells under hypoxia is in agreement with other reported studies.[44–47] Subarsky et al.[44] reported that cancer cell invasion was increased due to hypoxia of ≤ 5% oxygen tension, and Voss et al.[45] reported a 1.5 fold increase in the cell locomotion when the cells were incubated under hypoxic conditions of 1% oxygen tension. Furthermore, average speed of the cancer cell migration was calculated every hour (Fig. 4(d)), resulting in 1.5-fold increase by hypoxia on average. Our measurements of the migration speed in the 3D matrix agree well with previous reports under static conditions.[39]

To confirm that hypoxia associated signalling pathways are activated in our device under hypoxia, we performed immunostaining against HIF-1α and found an increase of HIF-1α expression in the cancer cells compared to normoxia (Fig. S8).[43,48, 49] A 1.7-fold increase in nuclear localization of HIF-1α in hypoxia compared to normoxia was detected, while we also observed a significantly higher increase (5.1-fold) under $CoCl_2$ stimulation (100μM). This increase in nuclear localization of HIF-1α under hypoxic conditions suggests increased activation of pathways controlled the HIF-1 transcription factor, which can result in enhanced tumor invasiveness[43], and thus may explain the observed difference in Fig. 6.

The *in vivo* oxygen tension in breast cancers was measured by Vaupel et al.[50] The median value of the oxygen tension was 30 mmHg (~ 4%), compared to 65 mmHg in normal breast tissue. Oxygen tension created in cell migration experiment was therefore appropriate to study the hypoxic effect on cancer cell behaviour. These results demonstrate the potential of our microfluidic device for the study of cell behaviour under controlled hypoxic conditions. An interesting direction for future work is the investigation of tumor cell directional migration under oxygen gradients.

Conclusions

This study reports a novel design of a microfluidic device for the culture of cells in a 3D hypoxic environment. Various parameters for defining the characteristics of the microfluidic device were optimised by numerical simulations to achieve a desired level of oxygen tension. The device was successfully validated, exhibiting a reasonably uniform low oxygen tension or an oxygen gradient across the gel region. The microfluidic device allowed for real-time imaging of human breast cancer cell migration in a 3D environment. Quantification of the cell trajectories demonstrated an enhanced migration of the cells in hypoxia in comparison to normoxia, further verifying the hypoxic environment generated within the device. Prospective application of this device lies in the study of other hypoxia-correlated cellular behaviours, such as proliferation, angiogenesis, and metabolism.

Supplementary Material

Refer to Web version on PubMed Central for supplementary material.

Acknowledgments

The authors would like to thank Mr. Ran Li and Mr. Sebastien Uzel for the helpful suggestions; Dr. Young K. Park for help during the early device designs; Ms. Reiko Maehara for assistance in the numerical simulation of the microfluidic device. KF acknowledges the Japan Society for the Promotion of Science for their funding under Young Researcher Overseas Visits Program for Vitalizing Brain Circulation. Support from the Singapore-MIT Alliance for Research and Technology (RK, CJO and YL) is also gratefully acknowledged.

Notes and references

1. Mohyeldin A, Garzon-Muvdi T, Quinones-Hinojosa A. Cell Stem Cell. 2010; 7:150–161. [PubMed: 20682444]
2. Studer L, Csete M, Lee SH, Kabbani N, Walikonis J, Wold B, McKay R. J Neurosci. 2000; 20:7377–7383. [PubMed: 11007896]
3. Horie N, So K, Moriya T, Kitagawa N, Tsutsumi K, Nagata I, Shinohara K. Cell Mol Neurobiol. 2008; 28:833–845. [PubMed: 18236013]
4. Bussink J, Kaanders J, Strik AM, Vojnovic B, van der Kogel AJ. Radiat Res. 2000; 154:547–555. [PubMed: 11025651]
5. Hockel M, Vaupel P. J Natl Cancer Inst. 2001; 93:266–276. [PubMed: 11181773]
6. Cairns RA, Kalliomaki T, Hill RP. Cancer Res. 2001; 61:8903–8908. [PubMed: 11751415]
7. Subarsky P, Hill RP. Clin Exp Metastasis. 2003; 20:237–250. [PubMed: 12741682]
8. Allen CB, Schneider BK, White CW. Am J Physiol-Lung C. 2001; 281:L1021–L1027.
9. Oppegard SC, Nam KH, Carr JR, Skaalure SC, Eddington DT. PLoS One. 2009; 4:e6891. [PubMed: 19727397]
10. Lo JF, Sinkala E, Eddington DT. Lab Chip. 2010; 10:2394–2401. [PubMed: 20559583]
11. Vickerman V, Blundo J, Chung S, Kamm R. Lab Chip. 2008; 8:1468–1477. [PubMed: 18818801]
12. Kim L, Toh YC, Voldman J, Yu H. Lab Chip. 2007; 7:681–694. [PubMed: 17538709]
13. Chung S, Sudo R, Zervantonakis IK, Rimchala T, Kamm RD. Advanced Materials. 2009; 21:4863–4867. [PubMed: 21049511]
14. Kothapalli CR, van Veen E, de Valence S, Chung S, Zervantonakis IK, Gertler FB, Kamm RD. Lab Chip. 2011; 11:497–507. [PubMed: 21107471]
15. Das SK, Chung S, Zervantonakis I, Atnafu J, Kamm RD. Biomicrofluidics. 2008; 2:034106.
16. Polacheck WJ, Charest JL, Kamm RD. Proc Natl Acad Sci U S A. 2011; 108:11115–11120. [PubMed: 21690404]
17. Zervantonakis IK, Hughes-Alford SK, Charest JL, Condeelis JS, Gertler FB, Kamm RD. Proc Natl Acad Sci U S A. 2012
18. Chung S, Sudo R, Vickerman V, Zervantonakis IK, Kamm RD. Ann Biomed Eng. 2010; 38:1164–1177. [PubMed: 20336839]
19. Sudo R, Chung S, Zervantonakis IK, Vickerman V, Toshimitsu Y, Griffith LG, Kamm RD. Faseb J. 2009; 23:2155–2164. [PubMed: 19246488]
20. Zervantonakis IK, Kothapalli CR, Chung S, Sudo R, Kamm RD. Biomicrofluidics. 2011:5.
21. Chen YA, King AD, Shih HC, Peng CC, Wu CY, Liao WH, Tung YC. Lab Chip. 2011; 11:3626–3633. [PubMed: 21915399]
22. Vollmer AP, Probstein RF, Gilbert R, Thorsen T. Lab Chip. 2005; 5:1059–1066. [PubMed: 16175261]
23. Nock V, Blaikie RJ, David T. Lab Chip. 2008; 8:1300–1307. [PubMed: 18651072]
24. Lam RHW, Kim MC, Thorsen T. Anal Chem. 2009; 81:5918–5924. [PubMed: 19601655]
25. Skolimowski M, Nielsen MW, Emneus J, Molin S, Taboryski R, Sternberg C, Dufva M, Geschke O. Lab Chip. 2010; 10:2162–2169. [PubMed: 20571689]
26. Mehta G, Mehta K, Sud D, Song JW, Bersano-Begey T, Futai N, Heo YS, Mycek MA, Linderman JJ, Takayama S. Biomed Microdevices. 2007; 9:123–134. [PubMed: 17160707]
27. Provin C, Takano K, Yoshida T, Sakai Y, Fujii T, Shirakashi R. Biomed Microdevices. 2009; 11:485–494. [PubMed: 19082898]

28. Adler M, Polinkovsky M, Gutierrez E, Groisman A. Lab Chip. 2010; 10:388–391. [PubMed: 20091013]
29. Domansky K, Inman W, Serdy J, Dash A, Lim MH, Griffith LG. Lab Chip. 2010; 10:51–58. [PubMed: 20024050]
30. Polinkovsky M, Gutierrez E, Levchenko A, Groisman A. Lab Chip. 2009; 9:1073–1084. [PubMed: 19350089]
31. Sinkala E, Eddington DT. Lab Chip. 2010; 10:3291–3295. [PubMed: 20938500]
32. Barbari TA, Koros WJ, Paul DR. J Polym Sci Pol Phys. 1988; 26:709–727.
33. Bae SY, Cho DH, Kim HT, Kumazawa H. Korean J Chem Eng. 1994; 11:127–130.
34. Netti PA, Guaccio A, Borselli C, Oliviero O. Biomaterials. 2008; 29:1484–1493. [PubMed: 18191194]
35. Taylor DA, Davis BH, Schroeder T, Yarmolenko PS, Guilak F, Dewhirst MW. Ann Biomed Eng. 2007; 35:1414–1424. [PubMed: 17417737]
36. Carrier RL, Rupnick M, Langer R, Schoen FJ, Freed LE, Vunjak-Novakovic G. Tissue Eng. 2002; 8:175–188. [PubMed: 12031108]
37. Acosta MA, Ymele-Leki P, Kostov YV, Leach JB. Biomaterials. 2009; 30:3068–3074. [PubMed: 19285719]
38. Charati SG, Stern SA. Macromolecules. 1998; 31:5529–5535.
39. Haessler U, Teo JCM, Foretay D, Renaud P, Swartz MA. Integr Biol-Uk. 2012; 4:401–409.
40. Burgess A, Vigneron S, Brioudes E, Labbe JC, Lorca T, Castro A. Proc Natl Acad Sci U S A. 2010; 107:12564–12569. [PubMed: 20538976]
41. Zahorodny-Burke M, Nearingburg B, Elias AL. Chem Eng Sci. 2011; 66:6244–6253.
42. Meyer AS, Hughes-Alford SK, Kay JE, Castillo A, Wells A, Gertler FB, Lauffenburger DA. J Cell Biol. 2012; 197:721–729. [PubMed: 22665521]
43. Indelicato M, Pucci B, Schito L, Reali V, Aventaggiato M, Mazzarino MC, Stivala F, Fini M, Russo MA, Tafani M. J Cell Physiol. 2010; 223:359–368. [PubMed: 20112292]
44. Subarsky P, Hill RP. Clin Exp Metastas. 2008; 25:253–264.
45. Voss MH, Feldman DR, Motzer RJ. Expert Rev Anticancer Ther. 2011; 11:1091–1103. [PubMed: 21806332]
46. Mikhaylova M, Mori N, Wildes FB, Walczak P, Gimi B, Bhujwalla ZM. Neoplasia. 2008; 10:380–U385. [PubMed: 18392137]
47. Cronin PA, Wang JH, Redmond HP. BMC Cancer. 2010; 10:225. [PubMed: 20492653]
48. Flamant L, Notte A, Ninane N, Raes M, Michiels C. Mol Cancer. 2010:9. [PubMed: 20085644]
49. Moroz E, Carlin S, Dyomina K, Burke S, Thaler HT, Blasberg R, Serganova I. PLoS One. 2009:4.
50. Vaupel P, Schlenger K, Knoop C, Hockel M. Cancer Res. 1991; 51:3316–3322. [PubMed: 2040005]

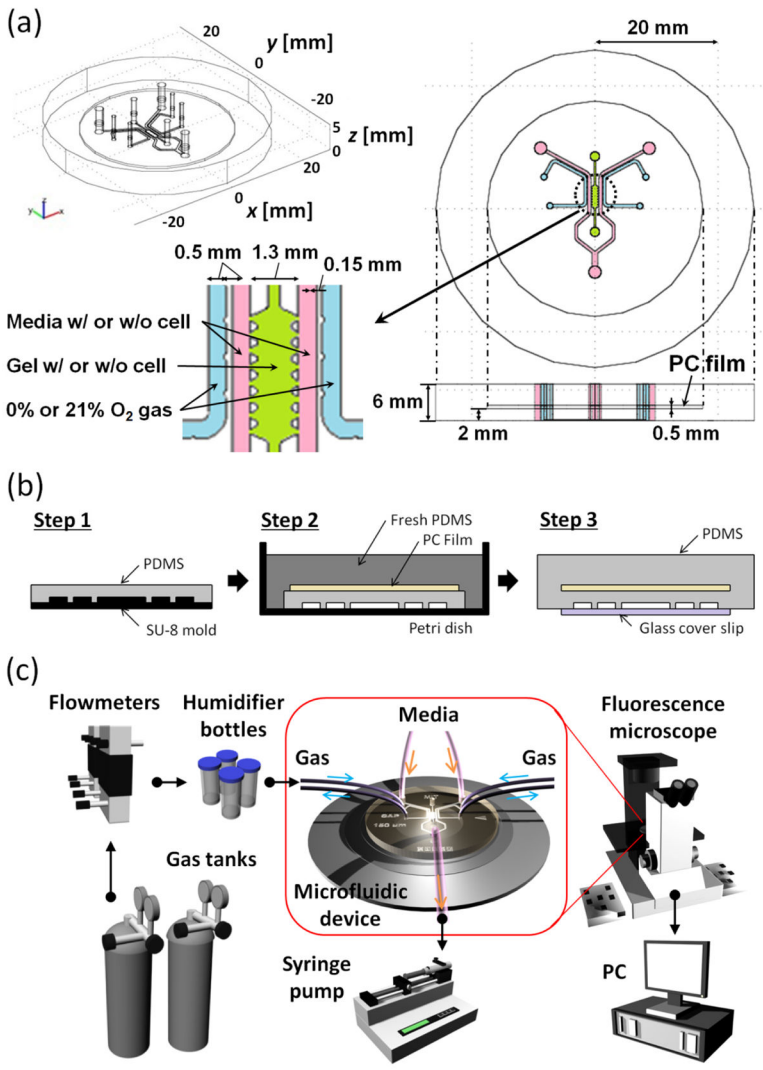

Figure 1.

Microfluidic device and experimental setup: (a) The design and configuration of a 6-mm-thick microfluidic device, within which a 0.5 mm polycarbonate (PC) film is embedded at the z = 2 mm mark, (b) a schematic of the device fabrication process, and (c) the experimental setup for hypoxia studies with cell culture.

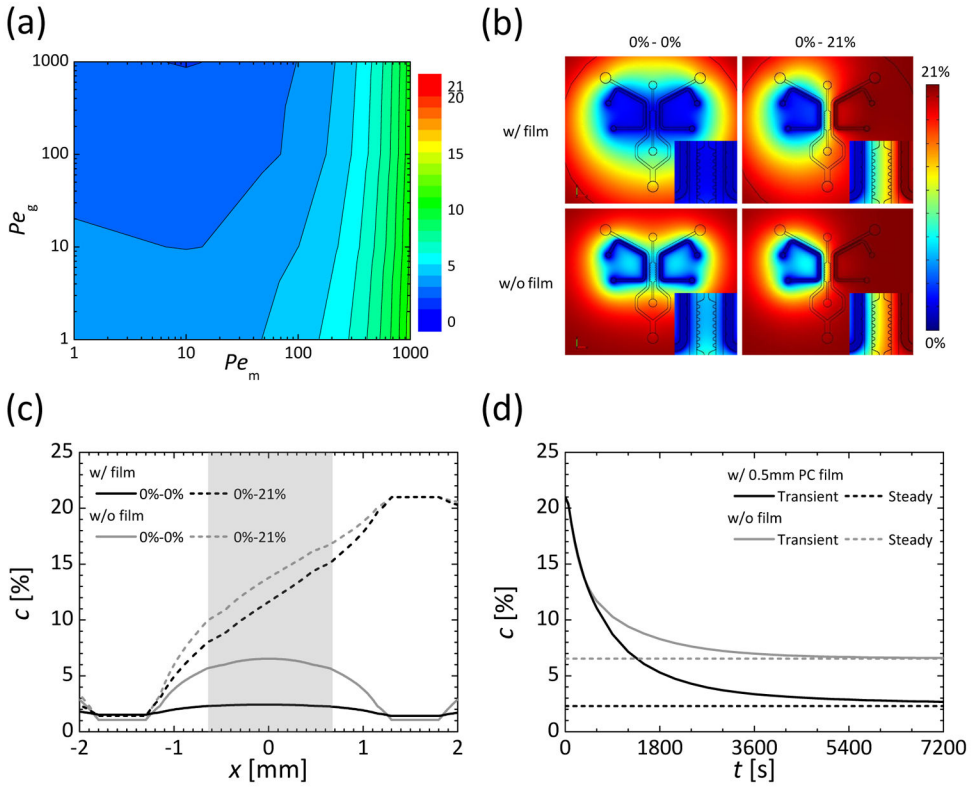

Figure 2.

Results in the numerical simulations of oxygen tension in the microfluidic device with/without a film of low diffusion coefficient of oxygen (D_{film} = 2.0×10^{-12} m^2/s), supplying 0% oxygen gas to both gas channels (0%-0%) or supplying it to the left-hand side gas channel, while supplying 21% oxygen gas to the right-hand side (0%-21%): (a) contour map of oxygen tension at the center of the gel region on a glass cover slip, (*x*, *y*, *z*) = (0 m, 1.975×10^{-3} m, 1×10^{-6} m), in the microfluidic device with the film with a combination of Péclet numbers for media and gas flow in the 0%-0% case, (b) steady oxygen tension on a crosssection (*z* = 1.0×10^{-6} m) and (c) the profile across the middle of the gel region (gray shaded zone), (*y*, *z*) = (1.975×10^{-3} m, 1×10^{-6} m) at media and gas flow rates of (Pe_m, Pe_g) = (10, 100), and (d) the transient change of oxygen tension at the center of the gel region.

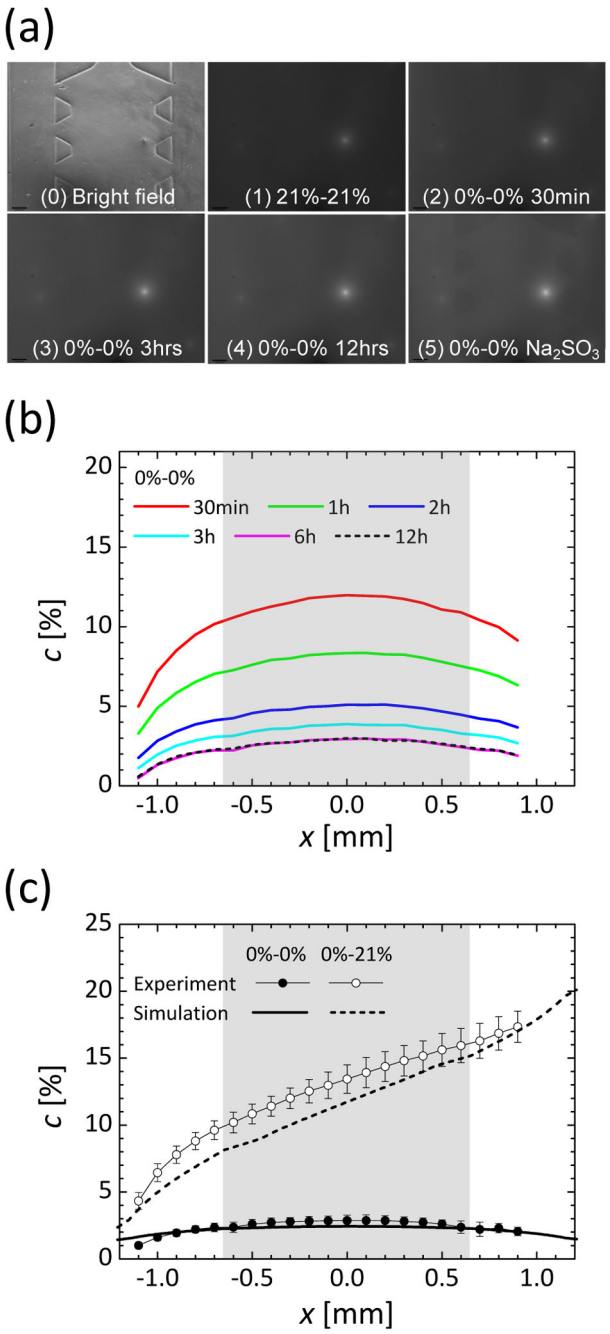

Figure 3.

Results in the validation experiment: (a) a set of bright field and fluorescence microscope images of the microfluidic device in various conditions, and (b) transient oxygen tension profiles across the gel region (gray shaded zone) after supplying 0% oxygen gas to both gas channels (0%-0%), and (c) steady oxygen tension profiles 12 hrs after supplying 0% oxygen gas to both gas channels (0%-0%) or supplying it to the left-hand side gas channels, while supplying 21% oxygen gas to the right-hand side (0%-21%). Each oxygen tension profile does not change after six hrs. Error-bars represent standard deviation.

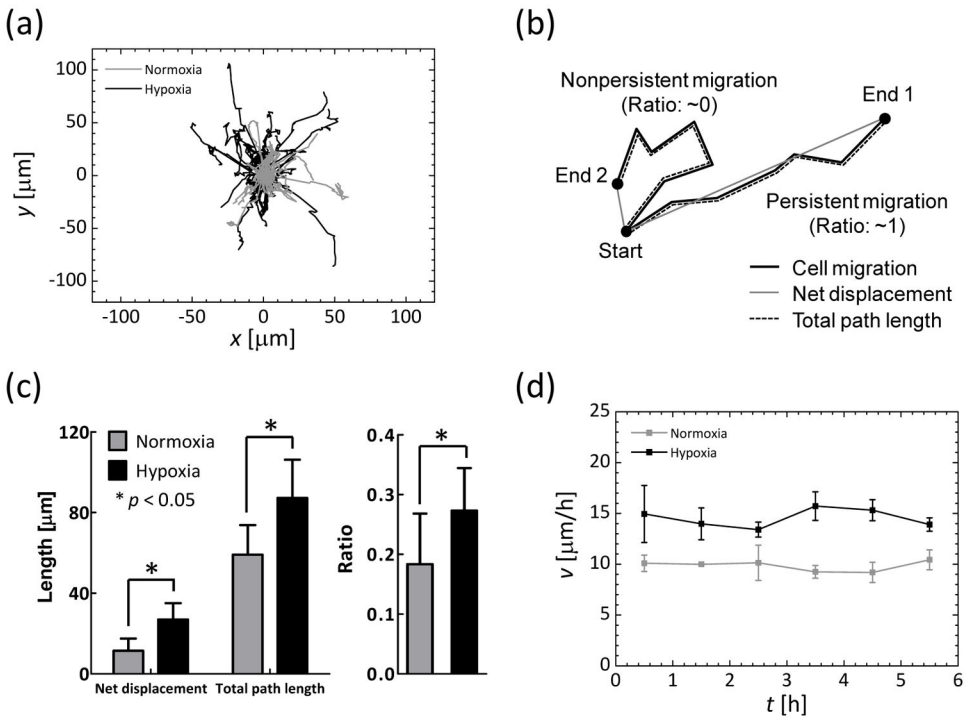

Figure 4.

Cancer cell migration under normoxia and hypoxia for six hrs: (a) trajectories of 35 cells in one device, (b) definition of metrics, (c) net displacement, total path length and their ratio (persistence) of cancer migration obtained with three microfluidic devices, and (d) the average speed of the migration. Error-bars represent standard deviation.

Table 1

Physical properties of each component and parameters for numerical simulations

	Gel	Media	PDMS	Gas	Film
Density, ρ [kg/m^3]	1.0×10^{3}	1.0×10^{3}		1	
Viscosity, μ [Pas]	1.0×10^{-3}	1.0×10^{-3}		1.0×10^{-5}	
Diffusivity of oxygen, D [m^2/s]	2.0×10^{-9}	2.0×10^{-9}	4.0×10^{-9}	2.0×10^{-5}	2.0×10^{-9} – 2.0×10^{-12}
Péclet number, Pe		0 – 1,000		0 – 1,000	
Average velocity, U [m/s]		0 – 4.0×10^{-3}		0 – 40	
Flow volume, Q [ml/min]		0 –1.8×10^{-2}		0 –1.8×10^{2}	
Oxygen tension, c [%]		21		0 or 21	

Table 2

Conditions for validation experiment

Procedure	O_2 in gas (Pe_g = 100)		Media (Pe_m)	Gel region	Duration
	L	R			
Validation experiment					
1. Calibration of 21% oxygen	21%	21%	Water (10)	Water	>30 min
2. Uniform hypoxia	0%	0%	Water (10)	Water	12 hrs
3. Oxygen gradient	0%	21%	Water (10)	Water	12 hrs
4. Calibration of 0% oxygen	0%	0%	Na_2SO_3 (0)	Na_2SO_3	>30 min
Cellular experiment					
A. Normoxia	21%	21%	DMEM (0)	Collagen type I gel w/cells	>8 hrs
B. Uniform hypoxia	0%	0%			>8 hrs